Thermal Transformation of $(NH_4)[Fe(AsO_4)F]$ Into the New Textural Porous Orthorhombic $Fe(AsO_4)$ Phase. Crystal Structures, Thermal Behavior, and Spectroscopic and Magnetic Properties

Begoña Bazán,[†] José L. Mesa,*[,‡] José L. Pizarro,[†] Jesús Rodríguez-Fernández,[§] Jorge Sánchez-Marcos,[§] Anna Roig,[||] Elies Molins,[||] María I. Arriortua,[†] and Teófilo Rojo*[,‡]

Departamento de Mineralogía y Petrología, and Departamento de Química Inorgánica, Facultad de Ciencia y Tecnologia, Universidad del País Vasco, Apdo. 644, E-48080 Bilbao, Spain, CITIMAC, Facultad de Ciencias, Universidad de Cantabria, 39005 Santander, Spain, and Instituto de Ciencia de Materiales de Barcelona (ICMAB-CSIC), Bellaterra, 08193 Spain

Received March 16, 2004. Revised Manuscript Received June 2, 2004

$(NH_4)[Fe(AsO_4)F]$ **1** has been synthesized under mild hydrothermal conditions. Single crystals of this phase heated under air atmosphere at 525 °C in a tubular furnace gave single crystals of the new polymorphous $Fe(AsO_4)$ **2**. The crystal structure of both compounds has been determined from X-ray single-crystal diffraction data. Compound **1** crystallizes in the orthorhombic $Pna2_1$ space group with unit-cell parameters of $a = 13.270(2)$ Å, $b = 6.629(1)$ Å, $c = 10.866(1)$ Å, $V = 955.8(2)$ Å^3, and $Z = 8$. Compound **2** belongs to the orthorhombic space group *Imam*, the unit cell parameters are $a = 13.468(2)$ Å, $b = 6.525(1)$ Å, $c = 10.768(2)$ Å, $V = 946.3(3)$ Å^3, and $Z = 12$. The crystal structure of compound **1** consists of a three-dimensional framework with chains formed by alternating $Fe(2)O_4F_2$ or $Fe(1)O_4F_2$ octahedra and $As(2)O_4$ or $As(1)O_4$ tetrahedra, respectively, linked by a common oxygen vertex. These chains run along the a and b axes of the crystal structure. The crystal structure of **2** is formed by a three-dimensional skeleton, constructed from sheets stacked along the [001] direction and interconnected by chains of alternating $Fe(2)O_6$ octahedra, sharing vertex with the $As(2)O_4$ tetrahedra. Transmission electronic microscopy of **2** indicates the existence of unconnected external and internal cavities with a BET surface area of 1.57(2) $m^2\ g^{-1}$. The diffuse reflectance spectra in the visible region show the forbidden electronic transitions characteristic of the d^5 high spin cations in slightly distorted octahedral geometry. The Mössbauer spectra of both phases at 300 K are characteristic of iron(III) cations. For each phase two sextets with similar isomer shifts and internal hyperfine fields of approximately 50 T were observed at 4.2 K. The ESR spectra from room temperature to 4.2 K remain isotropic with variation in temperature; the *g*-value being 1.99(1). The magnetic measurements at low temperatures indicate the predominance of antiferromagnetic interactions, with the Néel temperature being 68.0 and 54.5 K for compounds **1** and **2**, respectively. For both phases the existence of weak ferromagnetic components, giving rise to small hysteresis loops, was also detected at very low temperatures.

Introduction

The research on phosphate, phosphite, and arsenate materials with new open frameworks is currently in progress due to their potential applications in catalysis, gas separation, or as ion exchange.[1,2] Addition of fluoride anions into the reaction mixture, developed by Guth, Kessler, and Férey,[3] has led to the discovery of new microporous structural types, some of them exhibiting very large channels such as in cloverite,[4] ULM-5,[5a] MIL-31,[5b] MIL-46,[5c] and VSB-5.[5d] In these phases, the fluorine anions participate in the coordination sphere of the metal ion. A systematic study of the fluorine

* Authors to whom correspondence should be addressed. T.R. Phone: 34-946012458. Fax: 34-946013500. E-mail: qiproapt@lg.ehu.es. J.L.M. Phone: 34-946015523. Fax: 34-946013500. E-mail: qipmeruj@lg.ehu.es.

[†] Departamento de Mineralogía y Petrología, Universidad del País Vasco.

[‡] Departamento de Química Inorgánica, Universidad del País Vasco.

[§] CITIMAC, Universidad de Cantabria.

[||] Instituto de Ciencia de Materiales de Barcelona (ICMAB−CSIC).

(1) (a) Cheetham, A. K.; Ferey, G.; Loiseau, T. *Angew. Chem., Int. Ed.* **1999**, *38*, 3268.

(2) Davis, M. E. *Chem. Eur. J.* **1997**, *3* (11), 1745.

(3) (a) Guth, J. L.; Keesler, H.; Wey, R. *Stud. Surf. Sci. Catal.* **1986**, *28*, 121. (b) Ferey, G.; Loiseau, T.; Riou, D. In *Advanced Inorganic Fluorides: Synthesis, Characterization and Applications*; Nakajima, T., Zemva, B., Tressaud, A., Eds.; Elsevier Science: New York, 2000; Chapter 7.

(4) Estermann, M.; McCusker, L. B.; Baerlocher, C.; Merrouche, A.; Kessler H. *Nature* **1991**, *352*, 320.

(5) (a) Loiseau, T.; Ferey, G. *J. Solid State Chem.* **1994**, *111*, 403. (b) Sassoye, C.; Loiseau, T.; Taulelle, F.; Ferey, G. *Chem. Commun.* **2000**, 943. (c) Sassoye, C.; Marrot, J.; Loiseau, T.; Ferey, G. *Chem. Mater.* **2002**, *14*, 1340. (d) Guillou, N.; Gao, Q.; Forster, P. M.; Chang, J.-S., Nogues, M.; Park, S.-E.; Ferey, G.; Cheetham, A. K. *Angew. Chem., Int. Ed.* **2001**, *40*, 2831.

10.1021/cm040161s CCC: $27.50
Published on Web 11/13/2004

systems[6] has shown that the geometry of the structure-directing agent plays an important role for the attainment of three-dimensional open framework. It has also been observed that the ammonium groups from the organic molecules preferentially interact with the fluorine atoms of the framework via hydrogen bonds.

In the last few years, to stablish the relationships between the templates and the inorganic framework, the scientists working in this field have focused their attention on nitrogen rich molecules, such as ethylenediamine, 1,3-diaminopropane, piperazine, 1,4-diazabicyclo[2.2.2] octane, and 1,4,8,11-tetraazacyclotetradecane, etc.[7] In these organically templated materials the crystal structure collapses after losing the organic cation under heating. However, precursor materials with an open framework containing small particles, such as the ammonium cations, inside the inorganic skeleton could provide a new synthetic route to obtain new condensed materials by thermal treatment of these kinds of precursors. Furthermore, the use of both the ammonium cation and the fluorine anion together with an appropiate synthetic procedure could favor the attainment of new porous materials after thermal treatment of the resulting precursor. However, the $(NH_4)[Fe(PO_4)F]$ phosphate[8] does not exhibit this kind of behavior.

In this work we report on the hydrothermal synthesis of the $(NH_4)[Fe(AsO_4)F]$ phase and the new orthorhombic polymorphous $Fe(AsO_4)$ which exhibits a textural porosity. The new iron(III) arsenate phase is obtained in the form of single crystals by heating single crystals of ammonium fluoro-iron(III)-arsenate.[9] The crystal structures of both compounds were solved from single-crystal diffraction data. Mössbauer spectroscopy of both phases were performed at room temperature and 4.2 K showing in both cases two independent iron(III) sites magnetically ordered at low temperature. Magnetic and specific heat data indicate a complex antiferromagnetic behavior with a spin canting phenomenon at low temperatures.

Experimental Section

Synthesis and Characterization. $(NH_4)[Fe(AsO_4)F]$ was synthesized from a mixture in 20 mL of water of $FeCl_3 \cdot 6H_2O$ (0.204 mmol), As_2O_5 (1.5 mmol), and HF (57.5 mmol) and ammonium hydroxide to increase the pH up to 3.0. These reagents were stirred until homogeneity and sealed in a PTFE-lined stainless steel pressure vessel (filling factor 75%). After that the mixture was heated at 170 °C for 5 days, followed by slow cooling to room temperature. The pH of the mixture did not show any appreciable change during the hydrothermal reaction. Well-formed light-green single crystals were obtained. The composition of the compound, obtained by inductively coupled plasma atomic emission spectroscopy (ICP-AES), N-elemental analysis, and chemical analysis for fluorine content by using a selective electrode, is consistent with the formula $(NH_4)[Fe(AsO_4)F]$. Calcd: N, 6.0; As, 32.3; Fe, 24.1; F, 8.2. Found: N, 5.9; As, 32.0; Fe 23.9; F 7.7. Crystals of $(NH_4)[Fe(AsO_4)F]$ heated under air atmosphere at 525 °C in a tubular furnace yielded the $Fe(AsO_4)$ phase as brown single crystals. After thermal treatment, the total weight loss corresponded to 16.2%. Chemical analyses of this compound indicated the absence of $(NH_4)^+$ and F^- ions. A remarkable feature of the transformation between **1** and **2** compounds is that the crystalline state of the precursor is maintained during the thermal treatment. The densities, measured by flotation in mixtures of $CH_2I_2/CHBr_3$, were 3.27(2) and 2.79(5) g·cm^{-3} for compounds **1** and **2**, respectively.

Table 1. Crystal Data, Details of Data Collection, and Structure Refinement for $(NH_4)[Fe(AsO_4)F]$ and $Fe(AsO_4)$[a]

formula	$H_4AsFFeNO_4$	$AsFeO_4$
molecular weight (gmol^{-1})	231.8	194.8
crystal system	orthorhombic	orthorhombic
space group	$Pna2_1$ (no. 33)	*Imam* (no. 74)
a, Å	13.270(2)	13.468(2)
b, Å	6.629(1)	6.525(1)
c, Å	10.866(1)	10.768(2)
V^3	955.8(2)	946.3(3)
Z	8	12
$\rho_{calc.}$, g cm^{-3}	3.222	4.101
$F(000)$	888	1092
T, K	293(2)	293(2)
radiation, (Mo K), Å	0.71073	0.71073
μ(Mo Kα), mm^{-1}	9.971	15.014
limiting indices	$0 < h < 18$, $-9 < k < 9$, $-15 < l < 15$	$-16 < h < 16$, $-7 < k < 7$, $-13 < l < 13$
R [$I > 2(I)$]	R1 = 0.022, wR2 = 0.054	R1 = 0.018, wR2 = 0.040
R [all data]	R1 = 0.026, wR2 = 0.055	R1 = 0.022, wR2 = 0.041
GOF	1.082	1.002
$\Delta\rho_{max.}$ and $\Delta\rho_{min.}$, e Å^{-1}	0.673, −0.792	0.383, −0.849

[a] $R1 = [(|F_o| - |F_c|)]/|F_o|$; $wR2 = [[w(|F_o|^2 - |F_c|^2)^2]/[w(|F_o|^2)^2]]^{1/2}$; $w = 1/[^2|F_o|^2 + (xp)^2 + yp]$; where $p = [|F_o|^2 + 2|F_c|^2]/3$; $x = 0.027$, $y = 0.0$ for $(NH_4)[Fe(AsO_4)F]$; $x = 0.0324$, $y = 2.311$ for $Fe(AsO_4)$.

The infrared spectra of compounds **1** and **2** exhibit the bands corresponding to the vibrations of the ammonium cation and the $(AsO_4)^{3-}$ arsenate oxoanion.[10] The IR spectrum of **1** does not show bands above 3500 cm^{-1}, in accordance with the absence of $(OH)^-$ groups. The strong band centered at 3170 cm^{-1} corresponds to the stretching mode of the $(NH_4)^+$ group. The bending mode of this cation is observed at 1420 cm^{-1}. The positions of these bands in **1** are indicative of the existence of the ammonium cations,[10] which precludes the coordination of these cations to the inorganic $[Fe(AsO_4)]^-$ skeleton. The IR spectra of both compounds show the characteristic vibrational modes of the arsenate anion at similar frequencies. The asymmetrical stretching mode, ν_{as}(As−O), appears at frequencies 860, 830, and 810 cm^{-1} in **1** and at 935, 875, and 775 cm^{-1} in **2**. The symmetrical stretching band, ν_s(As−O), is detected at a frequency of 715 and 695 cm^{-1} for **1** and **2**, respectively. Finally, the asymmetrical deformation vibrations, δ_{as}(O−As−O), appear at 505 and 455 in **1**, and 490 and 450 cm^{-1} in **2**.

Single-Crystal X-ray Diffraction. Prismatic single crystals of compounds **1** and **2** with dimensions 0.3 × 0.2 × 0.1 and 0.25 × 0.2 × 0.1 mm, respectively, were carefully selected under a polarizing microscope and mounted on a glass fiber. The data collection was performed on Enraf-Nonius CAD4 and STOE IPDS automated diffractometers, for compounds **1** and **2**, respectively, with Mo Kα radiation. Details of crystal data, intensity collection, and some features of the structure refinement are reported in Table 1. It is important to emphasize the big difference between the experimental (2.79(5) gr/cm^3)

(6) (a) Ferey, G.; *J. Fluorine Chem.* **1995**, *72*, 187. (b) Ferey, G. *C. R. Acad. Sci. Paris Ser. IIc* **1998**, *1*, 1.

(7) (a) Fernandez, S.; Mesa, J. L.; Pizarro, J. L.; Lezama, L.; Arriortua, M. I.; Olazcuaga, R.; Rojo, T. *Chem. Mater.* **2000**, *12*, 2092. (b) Cavellec, M.; Riou, D.; Greneche, J. M.; Ferey, G. *Inorg. Chem.* **1997**, *36*, 2187. (c) Luo, S.-H.; Jiang, Y.-C.; Wang, S.-L.; Kao, H.-M.; Lii, K.-H. *Inorg. Chem.* **2001**, *40*, 5381. (d) Bazan, B.; Mesa, J. L.; Pizarro, J. L.; Garitaonandia, J. S.; Arriortua, M. I.; Rojo, T. *Solid State Sci.* **2003**, *5*, 1291. (e) Zhang, P.; Wang, Y.; Zhu, G.; Shi, Z.; Liu, Y.; Yuan, H.; Pang, W. *J. Solid State Chem.* **2000**, *154*, 368.

(8) Loiseau, T.; Calage, Y.; Lacorre, P.; Ferey, G. *J. Solid State Chem.* **1994**, *111*, 390.

(9) Bazan, B.; Mesa, J. L.; Pizarro, J. L.; Aguayo, T. A.; Arriortua, M. I.; Rojo, T. *Chem. Commun.* **2003**, 622.

(10) Nakamoto, K. *Infrared and Raman Spectra of Inorganic and Coordination Compounds*; John Wiley & Sons: New York, 1997.

and calculated (4.101 gr/cm^3) density values for compound **2**. This discrepancy suggests the existence of a porous nature for the [$Fe(AsO_4)$] phase, probably originated by the synthesis procedure. This hypothesis will be corroborated later.

In total, 5285 reflections were measured for **1** in the 3.07° ≤ θ ≤ 29.96° range, with 2740 reflections being independent ($R_{int.}$ = 0.0172) and 2529 observed applying the criterion $I > 2\sigma(I)$. For **2**, 3756 reflections measured in the 4.74° ≤ θ ≤ 25.87° range gave rise to 484 independent reflections ($R_{int.}$ = 0.0424) and 432 observed with $I > 2\sigma(I)$. Corrections for Lorentz and polarization effects of compound **1** were done and also for absorption with the empirical ψ scan method[11] by using the XRAYACS program.[12] For compound **2** these corrections were carried out with the software of the STOE IPDS diffractometer[13] by using the XRED program.[14] The structures were solved by direct methods (SHELXS 97)[15] and refined by the full-matrix least-squares procedure based on F^2, using the SHELXL 97 computer program[16] belonging to the WINGX software package.[17] The scattering factors were taken from ref 18. All non-hydrogen atoms were assigned anisotropic displacement parameters. The unit-cell parameters of compound **1** are close to those found for the $KTiO(PO_4)$-type materials. Furthermore, the diffraction symbol suggests two possible space groups, the acentric $Pna2_1$ (abc, No. 33) or the centric *Pnam* (setting a-cb of the *Pnma* No. 62). Nevertheless, the crystal structure only can be solved in the acentric $Pna2_1$ group. After the refinement procedure, the presence of a high pseudosymmetry (PLATON program), that corresponds to the *Pnan* space group (setting a-cb of the standard group *Pnna* No. 52) was revealed. Even this crystal structure can be solved in either the $Pna2_1$ or the *Pnan* groups. When the refinement is performed in the acentric space group the ammonium cations are placed in two different crystallographic positions (R1 = 0.030). However, if the centric *Pnan* supergroup is used, the ammonium cations must be considered as disordered in two equivalent positions with occupancy factors of 50% (R1 = 0.053). Therefore, taking into account that the space group used to describe the $KTiO(PO_4)$-type structures is the acentric $Pna2_1$[8,19] we have considered the solution in this space group. The value of 0.51(2) obtained for the Flack parameter in the refinement of the structure was a clear indication for a racemic twinning in the crystal studied. Consequently, the final refinement was performed including a correction for twinning by inversion, obtaining values of R1 = 0.026 and BASF = 0.52(1). Concerning phase **2**, it is important to note that the unit cell parameters are very close to those of compound **1**. To compare the two crystal structures, we have used the nonstandard space group *Imam* (setting a-cb of the standard group *Imma*, No. 74). Furthermore, this choice allows us to reveal the group−subgroup relationship between *Imam* → *Pnan* (the group that describes the pseudosymmetry present in **1**) → $Pna2_1$. A simulation based on the single-crystal structures of phases **1** and **2** was in excellent agreement with the X-ray powder data, indicating the presence of pure phases with high crystallinity. Further details on the crystal structure investigation may be obtained from the CCDC on quoting the depository numbers 197 540 and 197 541. All drawings were made using ATOMS program.[20] Atomic coordinates are shown in Table 2.

Table 2. Fractional Atomic Coordinates and Equivalent Isotropic Displacement Parameters (Å^2 × 10^3) for $(NH_4)[Fe(AsO_4)F]$ 1 and $Fe(AsO_4)$ 2 (ESD in Parentheses)

	x	y	z	U_{eq}[a]	Wyckoff position
		Compound **1**			
As(1)	0.1845(1)	0.5051(1)	0.9598(1)	6(1)	4*a*
As(2)	−0.0003(1)	0.1776(1)	0.7063(1)	5(1)	4*a*
Fe(1)	0.1128(1)	−0.0009(1)	0.9582(1)	6(1)	4*a*
Fe(2)	0.2458(1)	0.2553(1)	0.7057(1)	6(1)	4*a*
F(1)	0.2231(2)	0.0448(5)	0.8358(2)	11(1)	4*a*
F(2)	0.2232(3)	−0.0326(5)	1.0839(2)	13(1)	4*a*
O(1)	0.2371(3)	0.0486(6)	0.5784(3)	13(1)	4*a*
O(2)	0.0999(2)	0.3287(3)	0.6883(3)	11(1)	4*a*
O(3)	0.1123(2)	0.3024(4)	0.9951(2)	11(1)	4*a*
O(4)	−0.0129(3)	0.0157(6)	0.5903(3)	11(1)	4*a*
O(5)	0.0120(2)	0.0364(7)	0.8347(3)	13(1)	4*a*
O(6)	−0.1057(2)	0.3153(3)	0.7244(3)	9(1)	4*a*
O(7)	0.2611(3)	0.4564(6)	0.8383(3)	12(1)	4*a*
O(8)	0.1108(2)	−0.2963(4)	0.9304(3)	13(1)	4*a*
N(1)	0.1031(3)	−0.3165(5)	0.5196(3)	24(1)	4*a*
N(2)	−0.1102(3)	0.7215(5)	0.7710(4)	33(1)	4*a*
		Compound **2**			
As(1)	0.1766(1)	1/2	0	6(1)	8*f*
As(2)	0	0.1808(1)	3/4	4(1)	4*e*
Fe(1	0.1138(1)	0	0	6(1)	8*f*
Fe(2)	1/4	1/4	3/4	6(1)	4*d*
O(1)	0.2345(2)	0.0406(3)	0.6144(2)	8(1)	16*j*
O(2)	0.1098(2)	0.2944(4)	0.4684(2)	12(1)	16*j*
O(3)	0.1051(2)	0.3128(5)	3/4	9(1)	8*i*
O(4)	0	0.0260(5)	0.6228(2)	7(1)	8*h*

[a] $U_{eq} = (1/3)[U_{11}(aa^*)^2 + U_{22}(bb^*)^2 + U_{33}(cc^*)^2]$.

Physicochemical Characterization Techniques. The IR spectra (KBr pellets) were obtained with a Nicolet FT-IR 740 spectrophotometer in the 400−4000 cm^{-1} range. Thermogravimetric analyses were performed on a SDC 2960 simultaneous DSC−TGA TA instrument. Time-resolved X-ray thermodiffractometry was carried out in air atmosphere with a PHILIPS X'PERT automatic diffractometer (Cu Kα radiation) equipped with a variable-temperature stage (Anton Paar HTK16) and a Pt sample holder. Transmission electronic microscopy observations were carried out using a JEOL JSM-6400 instrument. Mössbauer spectra were obtained using a constant-acceleration Mössbauer spectrometer with a ^{57}Co/Rh source. The source was moved via triangular velocity waveform and the γ-counts were collected in a 512 multichannel analyzer. The data were folded, plotted, and fitted by a computer procedure. Velocity calibration was done using a 25-μm-thick metallic Fe foil, and the Mössbauer spectral parameters are given relative to this standard at room temperature. A Bruker ESP 300 spectrometer was used to record the ESR polycrystalline spectra from room temperature to 4.2 K. The temperature was stabilized by an Oxford Instrument (ITC 4) regulator. The magnetic field was measured with a Bruker BNM 200 gaussmeter and the frequency inside the cavity was determined using a Hewlett-Packard 5352B microwave frequency counter. Diffuse reflectance spectra were registered at room temperature on a Cary 2415 spectrometer in the 210−2000 nm range. Magnetic measurements on powdered sample were performed in the temperature range 2.0−300 K, at 0.1 T using a Quantum Design PPMS ac-magnetometer. The measurements were also performed at 0.05 and 0.01 T from 5.0 to 100 K using a Quantum Design MPMS-7 SQUID magnetometer. These values are in the range of linear dependence of magnetization vs magnetic field even at 5.0 or 2 K. Heat capacity measurements were carried out between 2 and 300 K by a relaxation method with a PPMS system and

(11) North, A. C. T.; Philips, D. C.; Mathews, F. S. *Acta Crystallogr.* **1968**, *A24*, 351−359.
(12) Chandrasekaran, A. XRAYACS: *Program for Single-Crystal X-ray Data Corrections*; Chemistry Department, University of Massachusetts: Amherst, 1998.
(13) *Stoe IPDS Software*, Version 2.87; Stoe & Cie: Darmstadt, Germany, 1998.
(14) *XRED*; Stoe & Cie: GmbH, Darmstadt, Germay, 1998.
(15) Sheldrick, G. M. *SHELXS 97, Program for the Solution of Crystal Structures*; University of Göttingen: Germany, 1997.
(16) Sheldrick, G. M. *SHELXL 97, Program for the Refinement of Crystal Structures*; University of Göttingen: Germany, 1997.
(17) Farrugia, L. J. WINGX, Version 1.63.02: An Integrated System of Windows Programs for the Solution, Refinement and Analysis of Single-Crystal X-ray Diffraction Data. *J. Appl. Crystallogr.* **1999**, *32*, 837−838.
(18) *International Tables for X-ray Crystallography*; Kynoch Press: Birmingham, England, 1974; Vol. IV, p 99.
(19) (a) Tordjman, I.; Masse, R.; Guitel, J. C. *Z. Kristallogr.* **1974**, *139*, 103. (b) Loiseau, T.; Paulet, C.; Simon, N.; Munch, V.; Taulle, F.; Ferey, G. *Chem. Mater.* **2000**, *12*, 1393.
(20) Dowty, E. *ATOMS: A Computer Program for Displaying Atomic Structures*; Shape Software: Kingsport, TN, 1993.

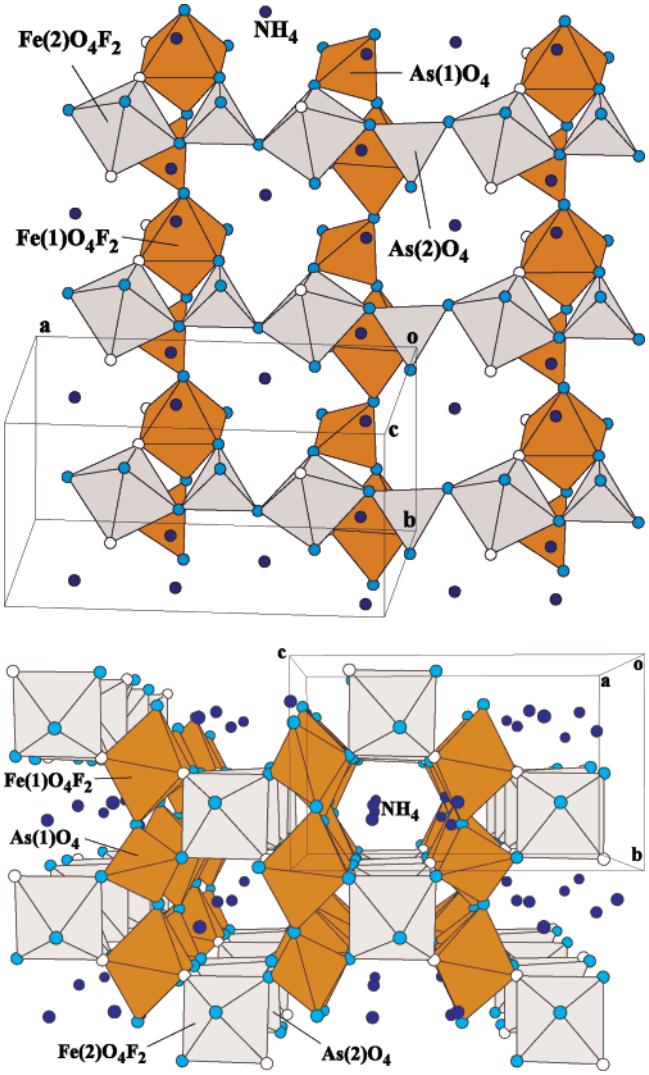

Figure 1. Polyhedral view of the crystal structure of **1** showing (a) the chains and (b) the channels along the |100| and |010| directions.

using a two tau model analysis. The sample was a plate of 0.3 mm thickness and 5 mg weight obtained by compressing the original powder.

Results and Discussion

Crystal Structure of the $(NH_4)[Fe(AsO_4)F]$ and $Fe(AsO_4)$ Compounds. The crystal structure of compound **1** consists of a three-dimensional framework constructed from corner-sharing FeO_4F_2 octahedra and AsO_4 tetrahedra. Chains formed by alternating Fe(2)-O_4F_2 or Fe(1)O_4F_2 octahedra and As(2)O_4 or As(1)O_4 tetrahedra, respectively, are running in the [100] and [010] directions and linked by a common oxygen vertex (Figure 1a). These chains are interconnected through the fluorine atoms belonging to the FeO_4F_2 octahedra. This architecture forms six-ring channels along the *a*- and *b*-axes in which the template ammonium cations are located in two different crystallographic positions (Figure 1b). The $(NH_4)^+$ groups compensate the anionic charge of the $[Fe(AsO_4)F]^-$ skeleton establishing hydrogen bonds with both the fluorine and oxygen atoms. This structural framework is similar to that of the KTiO-(PO_4)-type materials.[19a]

The Fe(1)O_4F_2 and Fe(2)O_4F_2 octahedra are linked together via the F(1) and F(2)-fluorine atoms. The Fe(1) cation of the Fe(1)O_4F_2 octahedron is bonded to the O(3), O(8) and O(4)^{i}, O(5)-oxygen atoms belonging to the As-(1)O_4 and As(2)O_4 tetrahedra, respectively, completing the hexa-coordination with two F(1) and F(2) atoms. The Fe−O bond distances are in the range 1.911(3)−2.050-(3) Å. The Fe−F bond lengths have a mean value of 2.007(3) Å. The *cis*-O−Fe(1)−O angles are in the 84.5(1)−93.3(1)° range, whereas the mean *trans*-O−Fe(1)−O angle is of 175.7(1)°. In the Fe(2)O_4F_2 octahedron the Fe(2) cation is bonded to the O(1), O(7) and O(2), O(6)^{iii} oxygen atoms from the As(1)O_4 and As(2)O_4 tetrahedra, respectively, with Fe−O bond lengths in the 1.951(3)−2.036(2) Å, range. The F(1) and F(2) atoms complete the coordination sphere around the Fe(2) cation at a mean distance of 1.991(3) Å. The *cis*-O−Fe(2)−O angles range from 85.1(2) to 95.1(2)°, and the *trans*-O−Fe(2)−O angles have a mean value of 177.3(2)°. The distortion of the Fe(1)O_4F_2 and Fe(2)O_4F_2 polyhedra, from an octahedron ($\Delta = 0$) to a trigonal prism ($\Delta = 1$), calculated by quantification of the Muetterties and Guggenberger description,[21] is $\Delta = 0.01$ and 0.03 for the octahedra belonging to the Fe(1) and Fe(2) cations, respectively. These values indicate a topology near to octahedron. The contact hydrogen distances established between the nitrogen atom of the ammonium cations and the fluorine and oxygen atoms of the $[Fe(PO_4)F]^-$ network exhibit a mean value of 2.78(1) Å.

The crystal structure of compound **2** shows a three-dimensional skeleton constructed from (001) sheets stacked along the [001] direction which are interconnected by chains of alternating Fe(2)O_6 octahedra sharing vertex with the As(2)O_4 tetrahedra (Figure 2a). The layers are formed by $Fe(1)_2O_{10}$ edge-sharing dimeric octahedra linked by common edges to the As(1)O_4 tetrahedra, which give rise to tetrameric units connected to each other by common oxygen vertex (Figure 2a). The six-ring channels observed in compound **1** are maintained along the *a*-axis of the three-dimensional network of compound **2**. The structure of this compound is similar to those observed for α-Cr(PO_4) and Rh(PO_4).[22]

The Fe(1) cations forming the Fe(1)O_6 octahedra are bonded to the O(1)^{i,ii} and O(2)^{i,ii} atoms from the As(1)-O_4 tetrahedron, and complete the hexacoordination with the O(4)^{i,ii} atoms belonging to the As(2)O_4 tetrahedron. The mean Fe(1)−O bond distance is 2.01(5) Å and the *cis*- and *trans*-O−Fe(1)−O angles range from 75.6(1) to 92.54(9)° and from 175.56(9) to 176.8(1)°, respectively. In the Fe(2)O_6 octahedron the metallic cation is bonded to the O(1) and O(3) atoms from the As(1)O_4 and As(2)-O_4 groups, respectively, with a mean bond length of 2.005(9) Å. The *cis*-O−Fe(2)−O angles are in the 86.9(1)−93.1(1)° range, whereas the *trans*-O−Fe(2)−O angles have a value of 180°. The distortion of these polyhedra, from an octahedron ($\Delta = 0$) to a trigonal prism ($\Delta = 1$), is $\Delta = 0.08$ and 0.008, for Fe(1) and Fe(2), respectively. These values indicate a topology near to octahedron.[21]

(21) Muetterties, E. L.; Guggenberger, L. J. *J. Am. Chem. Soc.* **1974**, *96*, 1748.

(22) (a) Attfield, J. P.; Sleight, A. W.; Cheetham, A. K. *Nature* **1986**, *322*, 620. (b) Glaum, R.; Gruehn, R.; Moller, M. *Z. Anorg. Allg. Chem.* **1986**, *543*, 111. (c) Attfield, J. P.; Cheetham, A. K.; Cox, D. E.; Sleight, A. W. *J. Appl. Crystallogr.* **1988**, *21*, 452. (d) Rittner, P.; Glaum, R. *Z. Kristallogr.* **1994**, *209*, 162−169.

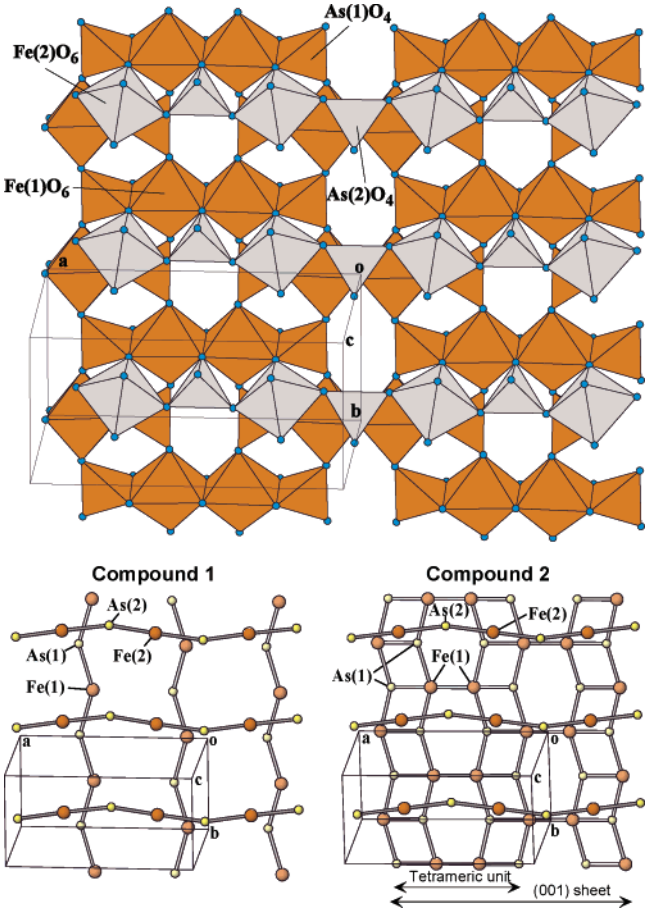

Figure 2. Polyhedral view of the crystal structure of **2** showing (a) the layers in the *ab*-plane and (b) relationship between the [100] and [010] chains in compound **1** and the [100] chains and the (001) sheets in compound **2**.

In both compounds, the arsenic atoms are in tetrahedral coordination with average As−O distances of 1.681(2) and 1.7(1) Å, for **1** and **2**, respectively. The O−As−O angles for both compounds are near 110°, as expected in the arsenate compounds with a sp^3 hybridization of the central arsenic atom.

From the structural point of view the two structures are very related. The precursor $(NH_4)[Fe(AsO_4)F]$ is formed by two types of $-FeO_4F_2-AsO_4-$ perpendicular chains, running along the [100] and [010] directions. However, for compound **2**, obtained after heating and elimination of the ammonium cations and fluoride ions, the chains along the [100] direction remain without modification but a duplication of the [010] chains takes place, giving rise to the (001) sheets formed by tetrameric units (Figure 2b). This feature is favored by the group−supergroup relationship between the *Pnan* pseudosymmetry of **1** and the *Imam* group of **2** (see the single-crystal X-ray diffraction section).

Thermal Behavior of the $(NH_4)[Fe(AsO_4)F]$ and $Fe(AsO_4)$ Compounds. The thermogravimetric analysis of **1** reveals a continuous weight loss of ca. 16.2% in the 180−500 °C temperature range. This loss has been attributed to the elimination of both the ammonium and fluorine ions of $(NH_4)[Fe(AsO_4)F]$ (calc. 16.0%) as NH_4F. The X-ray powder diffractogram of the inorganic residue obtained at 800 °C indicates the presence of the $Fe(AsO_4)$ monoclinic compound [$P2_1/n$ space group with a = 5.012(1) Å, b = 8.079(1) Å, c =7.564(1) Å, β = 104.5(1)°].[23]

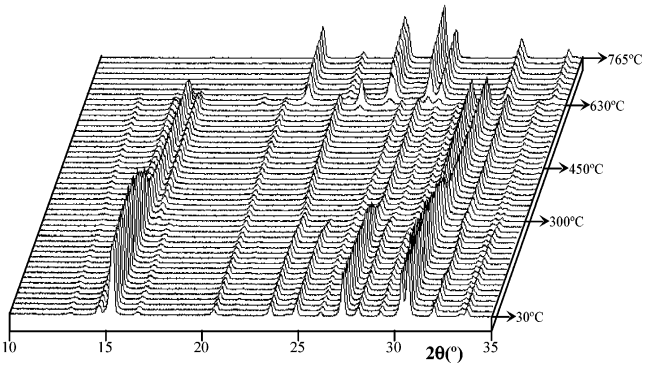

Figure 3. Thermodiffractograms of phase **1**. The temperatures at which the different transformations take place are marked.

The thermal behavior of compound **1** was also studied by using time-resolved X-ray thermodiffractometry in air atmosphere. The powder patterns were recorded in 2θ steps of 0.02° in the range $5 \le 2\theta \le 45°$, counting for 1 s per step and increasing the temperature at 5 °C·min^{-1} from room temperature up to 800 °C. Compound **1** is stable up to ca. 300 °C, as was also observed from thermogravimetric measurements, and the intensity of the monitored (011) peak at $2\theta = 15.62°$ remains practically unchanged (Figure 3). In the 450 to 630 °C range, and as a consequence of the loss of the ammonium and fluorine ions, the existence of the new orthorhombic $Fe(AsO_4)$ phase is observed. This phase transforms, at temperatures higher than 650 °C, into the monoclinic $Fe(AsO_4)$ compound,[23] in good agreement with the results obtained from the thermogravimetric study.

Transmission Electronic Microscopy and Nitrogen Sorption Measurements. To verify whether the loss of the ammonium and fluorine ions from phase **1** causes some superficial effect on the resulting compound **2**, TEM experiments were carried out. The TEM images of phase **2** obtained at different time steps of exposure of small single crystals of compound **1** to the source of electrons are shown in Figure 4. The pictures of phase **2** show that internal and external cavities without connection between them are generated. The maximum size is approximately 500 Å. These cavities are generated as a result of the loss of NH_4F in precursor **1**. Electron diffraction diagrams for **2** with a particle size of approximately 10−15 μm were recordered along two zone-axis being indexed with the *Imam* orthorhombic unit-cell obtained from X-ray diffraction data (Figure 5). This porosity is possibly formed by the migration of matter from some zones of compound **1** to form the crystal structure of **2** (leaving empty areas, e.g., porosity). This diffusion of matter would take place across the structural channels of the precursor, duplicating the [010] chains and forming the (001) sheets observed in **2** (see Figure 2b).

The textural porosity of compound **2** was confirmed by gas sorption isotherm experiments performed in liquid nitrogen. The compound exhibits capacity for N_2

(23) Powder Diffraction File−Inorganic and Organic, ICDD, File No. 21-190; ICDD: Newtown Square, PA, 1995.

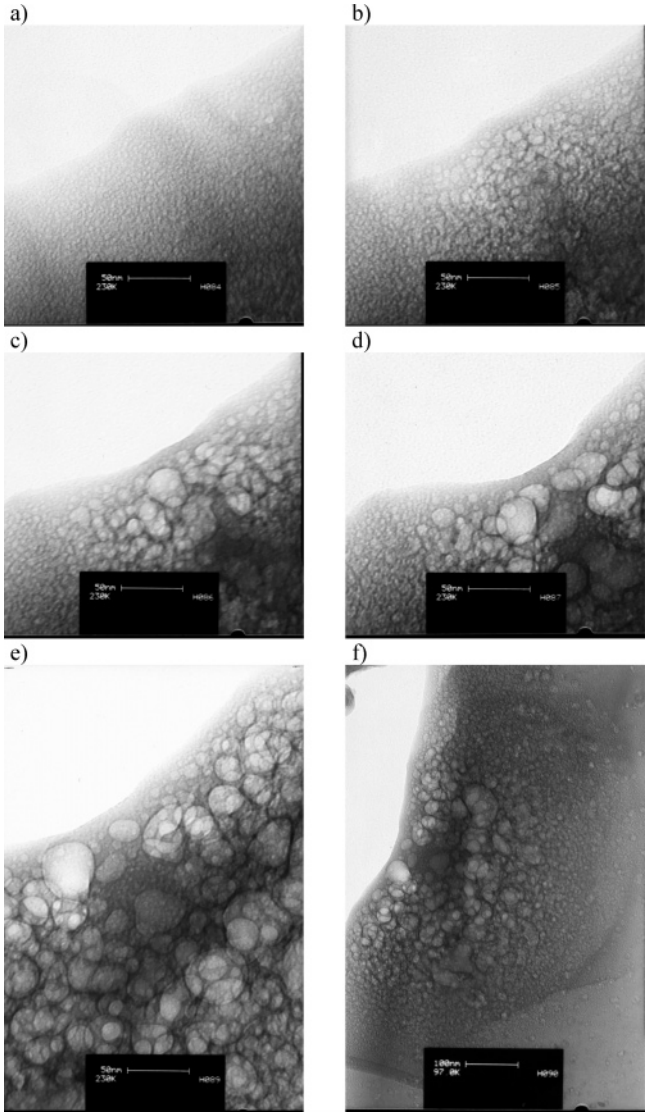

Figure 4. TEM images of compound **2** at different time steps of exposure of compound **1** to the source of electrons: (a) 0, (b) 15, (c) 45, (d) 90, (e) 300, and (f) 600 s.

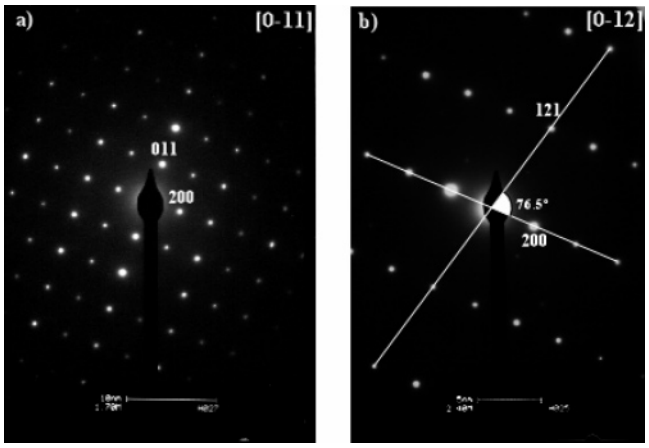

Figure 5. Electron diffraction diagram for **2**.

adsorption with a hysteresis upon desorption (Figure 6). The measured BET surface area is 1.57(2) $m^2\ g^{-1}$ and, assuming monolayer coverage by N_2, the Langmuir surface area is estimated to be 1.78(5) $m^2\ g^{-1}$. This small value can be associated with the existence of unconnected external and internal cavities in the surface of

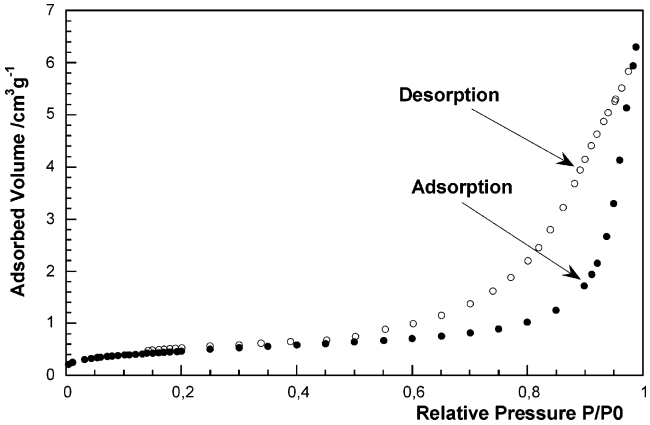

Figure 6. N_2 adsorption and desorption isotherms measured at 77 K.

phase **2** as was observed from the TEM photographs. The calculated average pore diameter is approximately 250 Å, in reasonable agreement with TEM measurements. The porous nature of compound **2**, observed by TEM and measured by BET, justifies the reduction of the theoretical density (4.101 g/cm^3) calculated by X-ray diffraction up to approximately $^2/_3$, to fit with the experimental data (2.79(5) g/cm^3).

UV−Visible and Mössbauer Spectroscopy. The diffuse reflectance spectrum of phase **1** shows bands at 13 005, 17 845, 23 285, and 26 130 cm^{-1}. However, for phase **2** only bands at 11 235 and 22 605 cm^{-1} are observed. The intensity of these bands is weak as expected for the spin forbidden transitions between the ground state $^6A_{1g}(^6S)$ and the excited levels $^4T_{1g}(^4G)$; $^4T_{2g}(^4G)$; $^4A_{1g}$,$^4E_g(^4G)$, and $^4T_{2g}(^4D)$ of a d^5-high spin cation in regular octahedral symmetry.[24] The Dq and Racah (B and C) parameters were calculated by using the energy expressions for an iron(III) high spin cation in octahedral geometry. The values obtained of Dq = 1090 cm^{-1}, B = 950 cm^{-1}, and C = 2760 cm^{-1} for **1** are in the range habitually found for the iron(III) cation in a slightly distorted environment.[24] The reduction of the B-parameter value with respect to that of the free ion (1150 cm^{-1}) in the ammonium compound is approximately 80%, suggesting a small covalent character of the Fe−O,F chemical bonds. For compound **2** the Dq and Racah parameters were not obtained due to absence of sufficient spectral bands.

Mössbauer spectra for compounds **1** and **2** at room temperature and 4.2 K are displayed in Figures 7 and 8, respectively.

Spectra recorded at 300 K (Figures 7a and 8a) show nonmagnetically split spectra. In both cases two subspectra of symmetric doublets were used in the fitting procedure with the NORMOS program (see Table 3).[25]

Isomer shift vales are consistent with the presence of high spin Fe(III) in octahedral environments and are similar to those observed for other iron containing phosphates.[26] Both compounds have very similar isomer

(24) Lever, A. B. P. *Inorganic Electronic Spectroscopy*; Elsevier Science Publishers B. V.: Amsterdam, The Netherlands, 1984.
(25) Brand, R. A.; Larner, J.; Herlach, D. M. *J. Phys.* **1984**, *F14*, 555.
(26) (a) Menil, F. *J. Phys. Chem. Solids* **1985**, *46*, 763. (b) Terminiello, L.; Mercader, R. C. *Hyperfine Interact.* **1989**, *50*, 651. (c) Beltran-Porter, D.; Olazcuaga, R.; Fournes, L.; Menil, F.; Le Flem, G. *Rev. Phys. Appl.* **1980**, *15*, 1115.

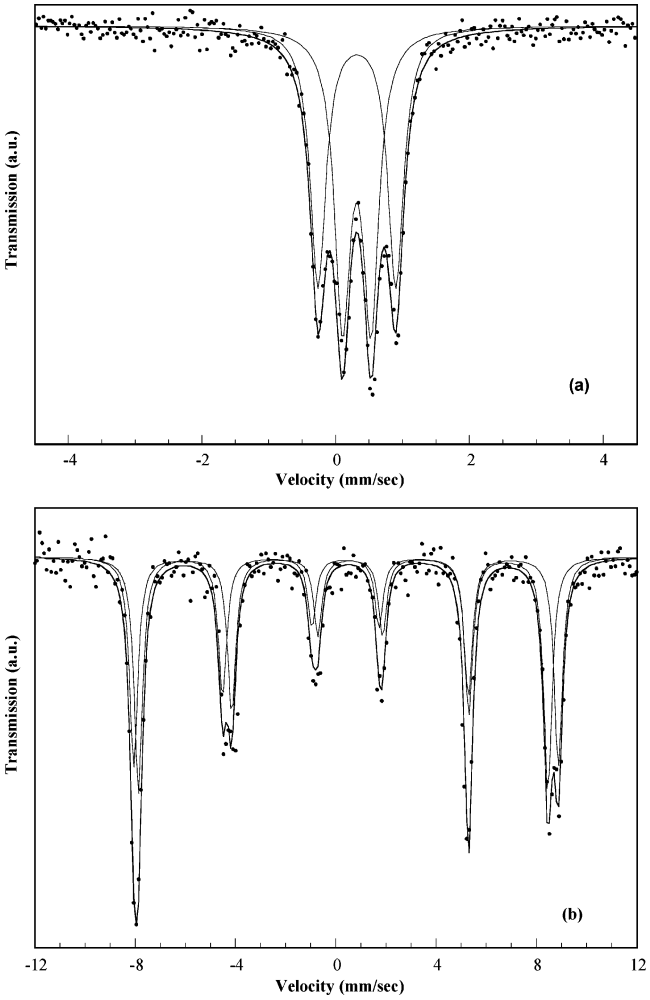

Figure 7. Mössbauer spectra of compound **1** at (a) 300, and (b) 4.2 K. Dots represent the experimental data, and solid lines represent the computer-fitted spectrum and the sub-spectra.

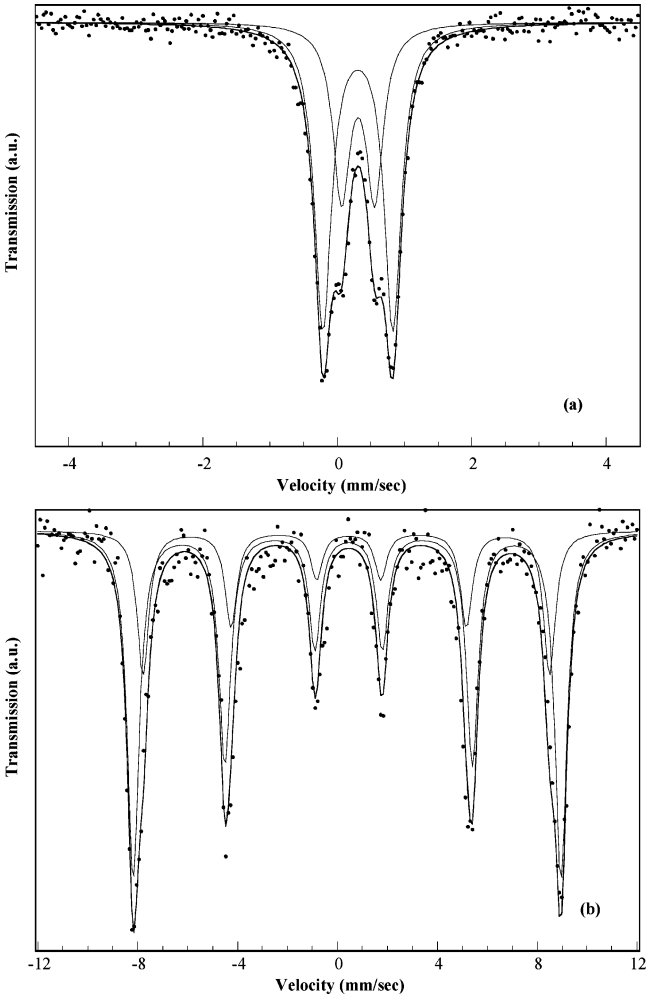

Figure 8. Mössbauer spectra of compound **2** at (a) 300, and (b) 4.2 K. Dots represent the experimental data, and solid lines represent the computer-fitted spectrum and the sub-spectra.

shift values indicating, as expected, the high ionicity of all the bonds for the two compounds.[26bc,27] Each sub-spectral doublet can be ascribed to one of the two nonequivalent crystallographic sites for iron by analyzing the Mössbauer spectra with the structural data. In the case of compound **2**, it can be seen from the structural data that the Fe(1) occupies an 8f site while the Fe(2) has a 4d site. In that case a univocal correspondence with the Mössbauer sub-spectra can be made. The sub-spectra with a Mössbauer resonant area of ~67% will correspond to Fe(1) and the sub-spectra with a resonant area of ~33% will correspond to Fe(2). This assignment is further confirmed by the quadrupolar splitting values. Fe(1) with a lager quadrupolar splitting occupies a less symmetric crystallographic position (8f) and Fe(2) occupies the more symmetric one (4d). Thus adscription is not so easy for compound **1** where both sites are in 4a general position. In this case the site with larger quadrupolar splitting can be assigned to Fe(1) where the two fluorine ions are adjacently located [angle F−Fe(1)−F = 86.3(8)°] while Fe(2) will correspond to the site with smaller quadrupolar splitting where the fluorinate ions are located opposite each other [angle F−Fe(2)−F = 176.0(2)°] creating a smaller electric field gradient over the iron site and consequently smaller quadrupolar splitting. This latter result is also related to the minor distortion observed in the $Fe(2)O_6$ octahedron. At 77 K the spectra (see Supporting Information) are very similar to those at 300 K, whereas at 4.2

Table 3. Hyperfine Parameters for the Fitting of the Mössbauer Spectra at 300, 77, and 4.2 K[a]

T (K)	position	δ (mm·s^{-1})	ΔEq (mm·s^{-1})	B_{HF} (T)	Γ (mm·s^{-1})	% Fe
			Compound **1**			
300	Fe(1)	0.394(8)	1.16(2)	0	0.285(4)	48(4)
	Fe(2)	0.391(1)	0.425(5)	0	0.284(5)	52(4)
77	Fe(1)	0.566(5)	1.05(1)	0	0.34(1)	49(4)
	Fe(2)	0.549(6)	0.436(8)	0	0.34(1)	51(4)
4.2	Fe(1)	0.48(1)	−0.02(2)	52.46(8)	0.40(2)	47(6)
	Fe(2)	0.51(1)	−0.28(2)	50.59(8)	0.40(2)	53(6)
			Compound **2**			
300	Fe(1)	0.382(2)	1.042(6)	0	0.307(8)	64(4)
	Fe(2)	0.385(4)	0.50(1)	0	0.307(8)	36(4)
77	Fe(1)	0.540(8)	1.04(4)	0	0.40(2)	67(6)
	Fe(2)	0.54(2)	0.52(4)	0	0.40(2)	33(6)
4.2	Fe(1)	0.497(1)	−0.06(1)	53.10(4)	0.57(2)	70(6)
	Fe(2)	0.40(1)	−0.09(2)	50.47(9)	0.57(2)	30(6)

[a] Isomer shift (δ) (relative to metallic iron), quadrupolar splitting (ΔEq), hyperfine field (B_{HF}), full width at half maximum (Γ), and ratio of iron(III) in each independent crystallographic site (%). Errors are given within and correspond to the last digit.

(27) Elbouaanani, L. K.; Malaman, B.; Gerardin, R. *J. Solid State Chem.* **1999**, *148*, 455.

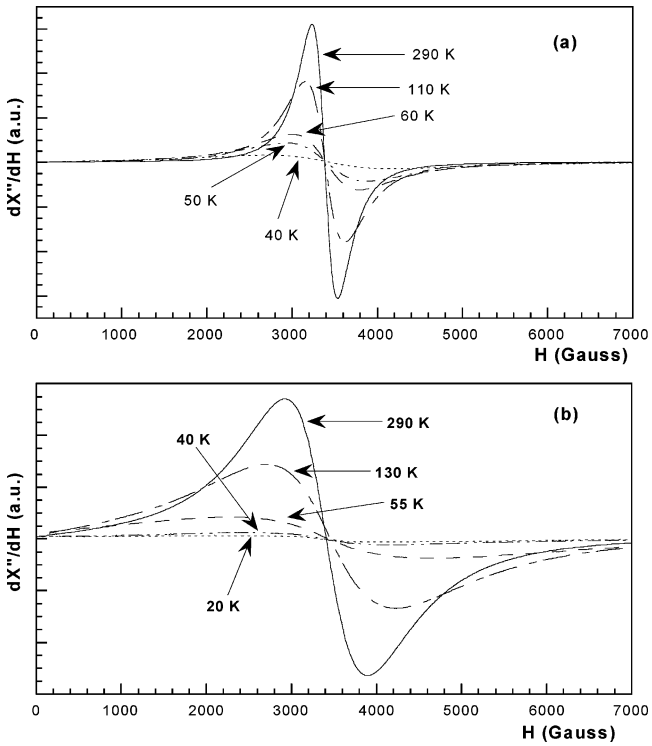

Figure 9. Powder X-band ESR spectra of (a) compound **1** and (b) compound **2** at different temperatures.

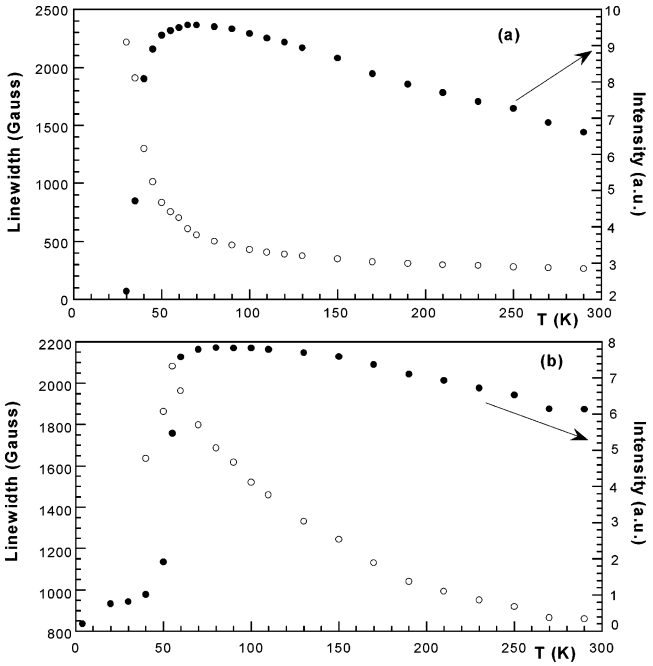

Figure 10. Temperature dependence of the intensity of the ESR signals and the line width curves for (a) compound **1** and (b) compound **2**.

K a good fit was achieved using two sextets (Figures 7b and 8b) confirming the magnetic order at low temperature observed from ESR and magnetic data.

Magnetic Study. The ESR spectra of **1** and **2** were recordered on powdered samples at X-band between 4.2 and 300 K (Figure 9).

The spectra remain essentially unchanged upon cooling the samples from room temperature to approximately 110 and 130 K for **1** and **2**, respectively (see Figures 9a and 9b). However, below these temperatures the line widths of the spectra broaden and lose intensity. The spectra of both compounds are isotropic with a g value of 1.99(1), which remains unchanged with variation in temperature. This g value is characteristic of octahedrally coordinated high spin Fe(III) ions.[28]

The thermal variations of the intensity and the line width of the signals, calculated by fitting the experimental spectra to Lorentzian curves, are displayed in Figure 10.

The intensity of the signal in both phases increases with decreasing temperature and reaches a maximum at around 70 and 65 K for compounds **1** and **2**, respectively. After these temperatures the intensity shows an abrupt decrease in both compounds, probably due to the predominance of antiferromagnetic interactions at low temperatures (see Figure 10a and b). In compound **1** (Figure 10a), the line width of the ESR signal slightly increases from room temperature to approximately 100 K, as a consequence of the dipolar homogeneous broadening.[29] When the temperature is further decreased the line width increases vigorously due to a strong spin correlation. However, for compound **2** (Figure 10b) the line width of the signals continuously increases from 300 K to approximately 60 K, and after that temperature shows a decrease at around 50 and 40 K. This fact is probably due to the long line width of the ESR curves at low temperatures, as shown in the spectra of Figure 10b, which precludes performing a good fit to Lorentzian curves.

Magnetic measurements of compounds **1** and **2** were carried out on powdered samples from room temperature to 2.0 K. The measurements performed at 1000 Oe in the zero field cooling (ZFC) and field cooling (FC) modes, show, in both cases, a similar thermal evolution of the molar magnetic susceptibility. Plots of χ_m and $\chi_m T$ curves are giving in Figure 11a and b, for **1** and **2**, respectively.

The molar magnetic susceptibility, χ_m, of both phases increases with decreasing temperature up to 58 and 54.5 K, temperatures at which the magnetic susceptibility shows a broad or sharp maximum in the case of compounds **1** and **2**, respectively. After these temperatures the susceptibility shows a strong decrease for compound **1** and slight decrease for compound **2** up to 7 and 28 K, respectively. Finally, the susceptibility slightly increases again in both compounds. These curves indicate the existence of antiferromagnetic interactions (T_N = 55 K in compound **2**) being of lower dimensionality in compound **1**. In this compound it is worth mentioning the change of curvature at T = 34 K, indicated by the vertical arrow in Figure 11a. This singularity is better observed in the derivative of the susceptibility, see inset in Figure 11a, where a sharp peak emerges at 34 K. In both compounds the susceptibility above $T \geq 150$ K is well described by a Curie–Weiss law, with a paramagnetic Curie temperature of approximately −280 and −320 K for compounds **1** and **2**, respectively. These results, together with the con-

(28) Bencini, A.; Gatteschi, D. *EPR of Exchange Coupled Systems*; Springer-Verlag: Berlin/Heidelberg, 1990.

(29) (a) Wijn, H. W.; Walker, L. R.; Daris, J. L.; Guggenheim, H. *J. Solid State Commun.* **1972**, *11*, 803. (b) Richards, P. M.; Salamon, M. B. *Phys. Rev. B* **1974**, *9*, 32. (c) Escuer, A.; Vicente, R.; Goher, M. A. S.; Mautner, F. *Inorg. Chem.* **1995**, *34*, 5707. (d) Cheung, T. T. P.; Soos, Z. G.; Dietz, R. E.; Merrit, F. R. *Phys. Rev. B* **1978**, *17*, 1266.

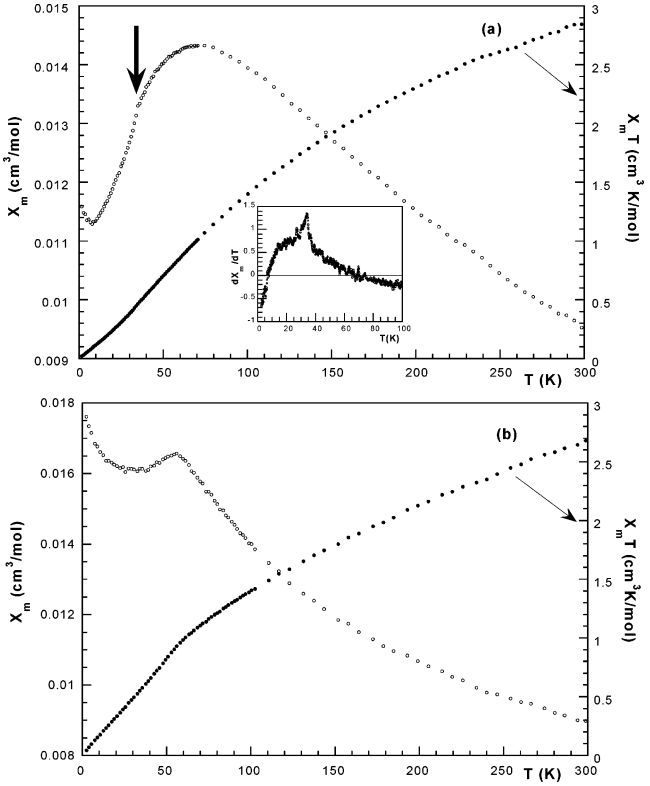

Figure 11. Thermal evolution of the molar magnetic susceptibility (χ_m) and the product $\chi_m T$, at 1000 Oe for (a) compound **1** and (b) compound **2**. The inset in (a) shows the derivative of the susceptibility ($d\chi_m/dT$).

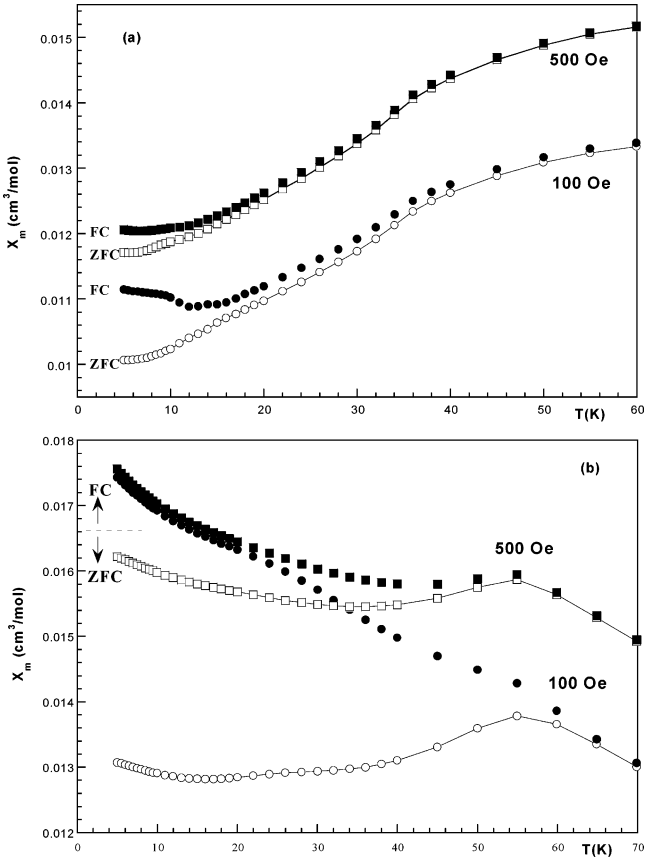

Figure 12. FC and ZFC magnetic susceptibility at 500 and 100 Oe for (a) compound **1** and (b) compound **2**.

tinuous decrease observed in the $\chi_m T$ products from 2.852 and 2.675 cm^{3}K/mol for **1** and **2**, respectively, at room temperature, to 0.023 and 0.035 cm^{3}K/mol at 2 K, are indicative of the predominance of strong antiferromagnetic interactions in both phases **1** and **2**.

The increase of the susceptibility at the lowest temperatures suggests the existence of a small ferromagnetic component. In the same way the thermal evolution of the χ_m measured at lower magnetic fields (500 and 100 Oe) in the FC and ZFC processes shows irreversibility, see Figure 12a and b. The irreversibility at 100 Oe starts at approximately 35 and 60 K for **1** and **2**, respectively, and appears at higher temperatures for higher magnetic fields. These irreversibilities suggest the existence of a weak ferromagnetic contribution at low temperatures in these phases.

Field-dependent magnetization data were recordered at 5 K in fields up to 70 kOe (Figure 13a and b). In both compounds, the magnetization does not saturate with field showing a quite linear behavior up to 70 kOe. In the low magnetic field region, see inset in Figure 13a and b, phase **2** shows a small hysteresis loop in which the values of the coercive field and remanent magnetization are, approximately, 67 Oe and 1.25 emu/mol, whereas the M vs H curve in compound **1** shows no hysteresis. These results confirm the existence of a weak ferromagnetic contribution intrinsic to the sample in phase **2**, probably due to a spin canting phenomenon. In addition, the nearly linear behavior of the M vs H curves up to 70 kOe reflect that the antiferromagnetic coupling persists up to this magnetic field; in fact, the magnetic moments at 70 kOe are 0.19 μ_B and 0.24 μ_B for phases **1** and **2**, respectively, being significantly lower than that expected for the saturation moment corresponding to $S = 5/2$. Furthermore, the absence of spin flopping or metamagnetism below 70kOe is in agreement with the strong anisotropy presented in these materials.[30]

Specific heat was measured by a relaxation method between 2 and 300 K in plates of about 5 mg obtained by compressing the original powder. The experimental data are depicted in Figure 14a and b. A small peak is observed in sample **1** at 34 K whereas a broad bump appears at 55 K in sample **2**. In both cases these anomalies correspond to the establishment of long-range magnetic order. For compound **2** the order temperature obtained from Cp corresponds to the temperature at which the peak in the susceptibility appears. However, in the case of compound **1** the anomaly in Cp does not correspond to the maximum in the susceptibility, but with a change of curvature (maximum in the derivative of the susceptibility). Therefore, these Cp results confirm both the existence of long-range magnetic order and the temperatures at which it occurs in both phases.

To obtain the magnetic specific heat (C_{mag}) we determine the phonon contribution and then subtract it from the experimental data. In the absence of nonmagnetic isomorphous compound, we should use a theroretical model to determine the phonon contribution, with the Debye model being the most common. However, due to the large differences in the atomic weights of the elements, more than one phonon spectra are expected.

(30) Cullity, B. D. *Introduction to Magnetic Materials*; Addison-Wesley: Reading, MA, 1972; p 239−241.

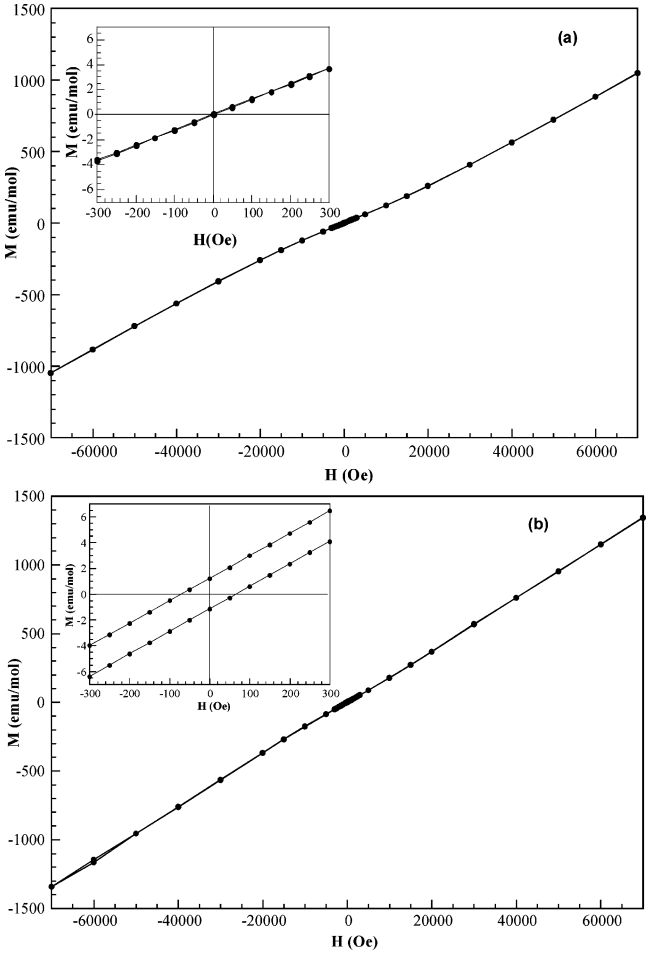

Figure 13. Hysteresis loops at 5 K for (a) compound **1** and (b) compound **2**.

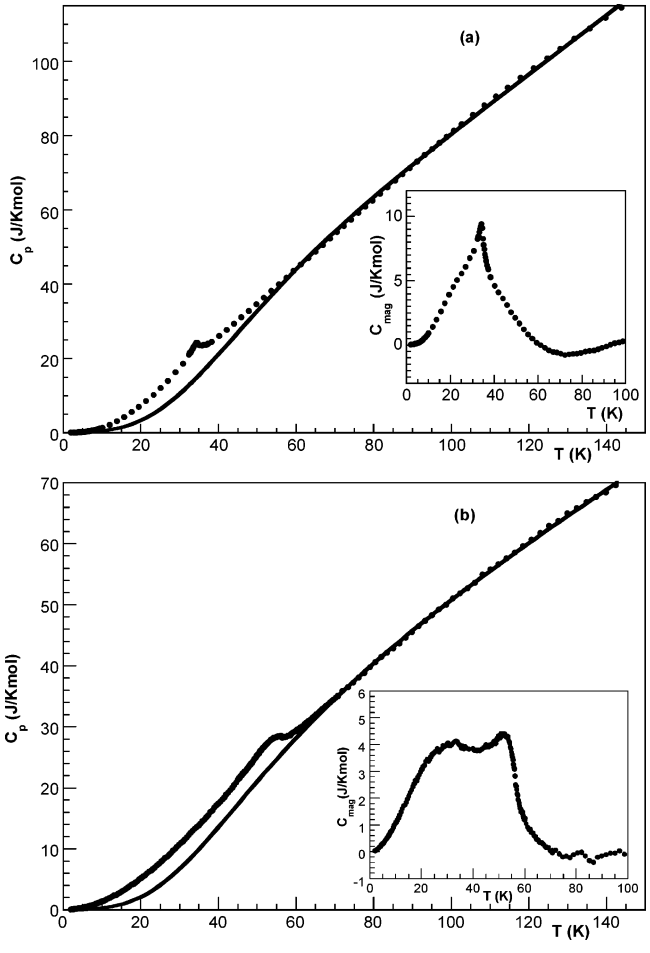

Figure 14. Specific heat between 1.8 and 150 K for (a) compound **1** and (b) compound **2**. Full points represent the experimental data and full line represents the estimated phonon contribution. The inset shows the calculated magnetic contribution.

The simplest way to solve this problem is to consider the existence of two phonon spectra. Therefore, if the number of atoms in the unit cell is N, we suppose n_A atoms with a Debye temperature Θ_A and $N - n_A$ atoms with a Debye temperature Θ_B. This approach has been used successfully in previous studies in other complex insulator materials.[31] The experimental data above the ordering temperature have been fitted to this phenomenological model. Continuous lines in Figure 14a and b show the best fit. The obtained parameters for compound **1** are $\Theta_A = 1018$ K, $\Theta_B = 260$ K, and $n_A = 8.4$ ions. In compound **2** the fitted parameters were $\Theta_A = 926$ K, $\Theta_B = 261$ K, and $n_A = 3.7$. The similarity between Θ_B values is in good agreement with the fact that both compounds have the same heavy elements. Furthermore, in compound **1**, in which the number of small elements increases, n_A increases in the same proportion, with the Θ_A values being slightly higher. The good quality of the fits as well as the coherence in the fitted parameters allow us to consider the calculated phonon heat capacity as a reasonable good approximation to the real one.

The estimated magnetic contributions are shown in the inset of Figure 14a and b for compounds **1** and **2**, respectively. In the first compound C_{mag} exhibits a relatively sharp peak centered at $T = 34.4$ K with a maximum value of ~10 J/Kmol; this peak resembles a λ-type anomaly characteristic of a 3D magnetic order. However, the C_{mag} of the second compound shows a broad bump with a maximum of ~4.3 J/Kmol and full width half-maximum of ~40 K. In this case, although small errors in the estimated phonon specific heat could contribute to the broadness of the C_{mag} peak, a broad magnetic contribution intrinsic to the sample should appear. This result contrasts with the well-defined peak in the susceptibility and suggests the existence of a complex magnetic behavior.

Taking into account the crystallographic results, the structure of compound **1** shows the existence of chains in which the metallic centers are linked through the fluorine ions with intermetallic Fe(1)−F(1), F(2)−Fe(2) angles of approximately 130°. In the crystal structure of phase **2** the connection between the metallic cations takes place through the oxygen atoms with intermetallic Fe(1)−O(4)−Fe(1) and Fe(1)−O(1)−Fe(2) angles of approximately 100 and 130°, respectively. These bond angle values together with those established by the arsenate anions to give rise to the three-dimensional network of these compounds should favor the antiferromagnetic interactions as was observed in other related compounds.[32] The complex magnetic behavior observed in both compounds could be induced by the existence of two sublattices with different magnetic moments anti-

(31) Rojo, J. M.; Mesa, J. L.; Lezama, L.; Pizarro, J. L.; Arriortua, M. I.; Rodriguez-Fernandez, J.; Barberis, G. E.; Rojo, T. *Phys. Rev. B* **2002**, *66* (9), 94406, and references therein.

ferromagnetically coupled in the presence of strong anisotropy. Powder neutron difffraction experiments are necessary in order to corroborate the existence of different magnetic sublattices which could explain the complex magnetic behavior and in particular the weak ferromagnetic contributions observed from the magnetic measurements at low temperatures in these compounds.

Concluding Remarks

Two new three-dimensional arsenates, $(NH_4)[Fe(AsO_4)F]$ **1** and $Fe(AsO_4)$ **2**, have been synthesized by using mild hydrothermal techniques and solid-state reaction in air atmosphere, respectively. The crystal structures of the two compounds are closely related. Compound **1** is made by two perpendicular chains along the [100] and [010] directions, and compound **2**, which was obtained by direct heating of single crystals of compound **1**, shows chains formed by tetrameric units from a duplication of the [010] chains maintaining invariable those corresponding to the [100] directions. The new orthorhombic $Fe(AsO_4)$ phase exhibits a textural porosity with unconnected external and internal cavities the maximum size of which is approximately 500 Å. Spectroscopic measurements confirm the existence of two kinds of d^5 high spin Fe(III) ions in the structure. The specific heat measurements exhibit a λ-type peak characteristic of a 3D magnetic order for compound **1**, but a broad bump is observed for compound **2**, indicating a more complex magnetic behavior of this compound. Both phases show the presence of long-range antiferromagnetic interactions being of lower dimensionality in compound **1**. The existence of weak ferromagnetic contributions has been also observed. Preliminary neutron diffraction measurements, performed on the D1B diffractometer at the ILL (Grenoble), indicate the existence of inconmensurable magnetic structures for **1** and **2**.

Acknowledgment. This work was financially supported by the Ministerio de Educación y Ciencia (PB97-0640; BQU2001-0678) and the Universidad del País Vasco/EHU (9/UPV00169.310-14199/2001; 9/UPV00130.310-13700/2001), which we gratefully acknowledge. B. Bazán thanks the Universidad del País Vasco/EHU for a fellowship.

Supporting Information Available: Listing of details of the X-ray single-crystal diffraction structural resolution, thermogravimetric curve for **1**, and Mössbauer spectra for **1** and **2** (pdf). Crystallographic information (cif). This material is available free of charge via the Internet at http://pubs.acs.org.

CM040161S

(32) Goodenough, J. B. *Magnetism and the Chemical Bond*; Interscience: New York, 1963.